

ARTICLE OPEN



Long-term aging of CVD grown 2D-MoS₂ nanosheets in ambient environment

Nitul S. Rajput¹, Ahmed Kotbi², Khaled Kaja³ and Mustapha Jouiad²✉

A chemically vapor deposited MoS₂ nanosheets (NSs) is aged in the laboratory at ambient and at 40% average humidity for ~36 months. Nanorods of few microns in length and few nanometers in diameter are found to grow from the MoS₂ seeds. They have been growing as a result of the chemical reaction between the MoS₂ NSs and ambient O₂ and moisture, they exhibit an amorphous phase structure in the stoichiometric form of MoO₃. Density functional theory simulations further reveal the role of H₂O and O₂ in the transformation of the MoS₂ NSs. The adsorption energy of O₂ molecules on the MoS₂ sites is $E_{\text{ad}} = -1.09$ eV as compared to lowest absolute $E_{\text{ad}} = -0.10$ eV of H₂O indicating the favorable adsorption of O₂ and subsequent Mo oxidation. This study provides valuable insight into the aging phenomenon of MoS₂ exposed to O₂ and moisture which might limit their application.

npj Materials Degradation (2022)6:75; <https://doi.org/10.1038/s41529-022-00288-4>

INTRODUCTION

Molybdenum disulfide (MoS₂) has emerged in the last decade as one of the most promising two-dimensional (2D) transition metal dichalcogenide (TMD) materials for its excellent mechanical and unique optical properties. This has spurred the interest around MoS₂ making it highly desirable for optoelectronic applications^{1–4}. Several attempts are currently in progress to build devices based on MoS₂ such as sensors, photodetectors, flash memories, batteries, field emitters, rectenna for energy harvesting, etc.^{5–10}. Additionally, the low frictional coefficient of MoS₂ triggered its use as a lubricant in aerospace-related applications¹¹. Nonetheless, prior to its implementation in realistic applications, it is necessary to evaluate its mechanical, chemical, and structural stability over a long period of time, mimicking the actual use of devices in ambient environment. In a study conducted by Budania et al.¹², the long-term (~7–8 months) stability of mechanically exfoliated MoS₂ flakes was inspected in air and vacuum. Small patches were observed on the flakes left in ambient air for about 55 days, whereas no change was identified for samples stored in vacuum. White patches were ascribed to oxidized MoS₂ sites with higher Mo concentration. In a separate study by Gao et al.¹³, the stability of MoS₂ and WS₂ exposed to ambient air (6–12 months) was investigated, suggesting the presence of a gradual oxidation of these compounds along with an extensive cracking and changes in their morphology. These transformations were attributed to the presence of oxygen and moisture in the environment leading to the oxidation of the flakes. Other authors ascribed the degradation of chemical vapor deposition (CVD) grown monolayer MoS₂ flakes to the presence of S vacancies¹⁴. These authors proposed the control of S defect density by tuning the CVD growth condition to ensure a long-term stability of the material.

It was also proposed that the aging effect can be avoided by capping the material with a protecting polymer layer. Besides, Yao et al.¹⁵ have reported that the preheating of a monolayer MoS₂ sample can accelerate its degradation process. In addition, the surface oxidation of MoS₂ was reported to evolve during the

sample exposure to moisture¹⁶. In this case, the oxidation process led to partial etching of the MoS₂ surface, which constitutes a very important finding since MoS₂ is considered as a potential water splitting catalyst. Thus, its instability in water could compromise its implementation in water splitting devices. Indeed, as reported earlier, the degradation of the film/flake quality can eventually affect the performance of their electrical, optical or tribological properties^{13,17,18}. Nonetheless, it is worth noting that the degradable nature of MoS₂ (or in general the TMD materials) could be held as a potential candidate for bioabsorbable electronics¹⁹.

Although reported investigations on the degradation of MoS₂ revealed very interesting findings, challenging the initial assumption of its stability in ambient environment, their extent has few limitations in different aspects. First, all reported modifications induced through aging on MoS₂ were studied for a relatively shorter amount of time. Even though changes have been identified, affecting the applicability of MoS₂, the aged material could be beneficial for other applications such as in bioabsorbable electronics¹⁹ or could be a potential candidate for charge storage²⁰, gas sensing²¹ or electromagnetic wave absorption²². Second, most of the available studies have mainly assessed the surface dependent structural modifications of MoS₂ layers. That is, the morphological state of surfaces showed the formation of cracks and oxidation-related patches determined by scanning probe microscopy methods. In addition, Raman spectroscopy and imaging, as well as XPS investigations were used to comprehend chemical changes associated with those observed in morphology. Nonetheless, comprehensive structural studies investigating the microscopic origins of aging mechanisms through depth profiles of MoS₂ structures remain lacking. In the light of these limitations, our work presents a longer-term aging (~36 months) study carried out on vertically oriented MoS₂ material grown by CVD. Lately, the vertically aligned MoS₂ NSs are gaining great interest, their sharp edges offer more exposed sites for increasing physical-chemical interactions, making them suitable for various applications such as

¹Advanced Materials Research Center, Technology Innovation Institute, P.O. Box 9639, Abu Dhabi, United Arab Emirates. ²Laboratory of Physics of Condensed Matter, University of Picardie Jules Verne, Scientifica Pole, 33 rue Saint-Leu, 80039 Amiens Cedex 1, France. ³Laboratoire National de métrologie et d'essais (LNE), 29 Av. Roger Hennequin, 78197 Trappes, France. ✉email: mustapha.jouiad@u-picardie.fr

optoelectronics²³, gas sensing²⁴, and field emission devices⁹. Moreover, the vertically oriented MoS₂ sheets are found to exhibit similar optoelectronic response as monolayer MoS₂⁴.

Interconnected MoS₂ nanosheets (NSs) were obtained by sulfurization process^{4,25} and then exposed to the laboratory environment for a period of ~3 years. Substantial modifications in the structural nature of the sample were observed, namely the “natural” growth of MoO_x nanorods formed over time. The microscopic mechanism behind such a remarkable aging effect has been investigated by cross-sectional transmission electron microscopy (TEM). Raman and XPS characterizations were also performed to reveal the chemical changes associated with this aging mechanism. We used density functional theory (DFT) calculations to investigate the origins of the aging process, which has been successfully correlated to experimental results. Based on these understandings, we have finally undergone an artificially induced aging of the MoS₂ NSs using electron beam irradiations to enhance chemical oxidation reactions. Interestingly, we succeeded in reproducing an aging effect in nanorods demonstrating the structural and crystalline changes. This work offers valuable means for the control of very long MoS₂ stability in ambient environment, which is intended to help improving functional devices’ nano-engineering strategies.

RESULTS

Structural characterization

Pristine MoS₂ NSs are shown in the SEM image in Fig. 1a. The pristine sample consisted of continuous and densely packed vertically oriented MoS₂ NSs, with a typical thickness of 5–20 nm, forming an interconnected network with a high degree of crystallinity, as demonstrated in our previous TEM study⁹. Exposed

edges of the vertically grown NSs presented a tip-like morphology exhibiting high performing field emitting properties⁹.

Micrographs depicted in Fig. 1b, c showcase the top and side views, respectively, of the same sample after being exposed to ambient environment conditions for a period of ~36 months. Imaging results clearly show overall morphology changes induced on the sample, where polygonal-shaped nanorods nucleate and grow from the MoS₂ NSs surface.

Nanorods are few tens of nm in diameter and few hundreds of nm to few microns in length. They are observed to nucleate and grow from the MoS₂ surface in a random orientation. Figure 2a shows the starting growth seeds of few typical nanorods, indicated by arrows pointing out their nucleation sites.

A cross-sectional view of a nanorod prepared using FIB milling process is shown in Fig. 2b. The measured height of the vertically oriented rod is 900 nm from the surface. The image provides a closer view on the intact nature of the nanorods with the MoS₂ surface.

To examine the nanorods composition, an ultra-thin cross-sectional sample was prepared and further investigated in a TEM microscope. The side view of a nanorod lying on the MoS₂ surface is exhibited in Fig. 3a. Four regions can be clearly distinguished in the TEM image including the SiO₂ substrate (region 1), Mo thin film (region 2) with a sulfurized portion (region 3), and the nanorod portion (region 4). A magnified image collected from the nanorod region 4 is shown in Fig. 3b. The corresponding FFT image is presented in the inset. The HRTEM and FFT images reveal a mostly amorphous form of the nanorods with negligible appearance of randomly distributed nanocrystals. The degree of nano crystallinity increases with the electron beam fluence, which is further discussed later. Additionally, energy dispersive spectroscopy (EDS) was performed on the four regions and results are shown in Fig. 3c. The EDS analysis suggests that molybdenum

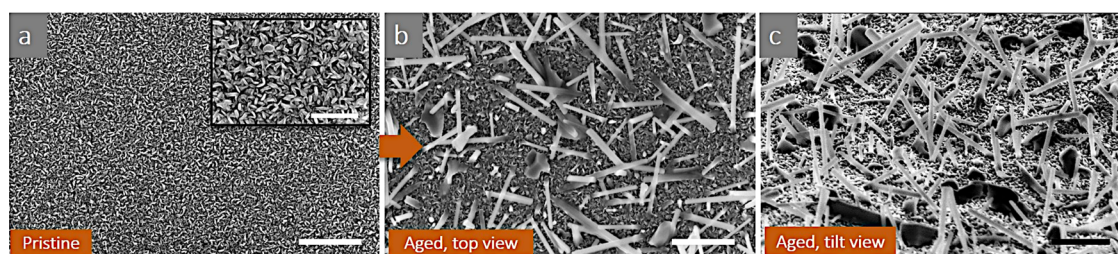


Fig. 1 Sample evolving morphology. **a** A top view SEM image of the grown MoS₂ sample (pristine); scale bar 1 μm; a magnified view is shown in the inset; scale bar = 300 nm. **b** Top view SEM image of the same sample after a long-term aging period of ~36 months. The formation of nanorods can be seen over the sample surface. **c** Tilt view of the sample indicating the randomly grown nanorods. Scale bars in **b** and **c** 1 μm.

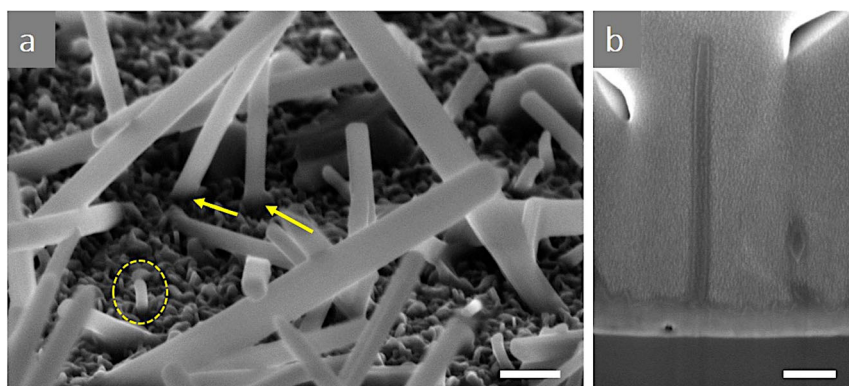


Fig. 2 Nucleation of nanorods. **a** SEM tilt view showcases the nucleation of the nanorods from the sample surface. The arrows indicate the nanorods seeds emanating from the MoS₂ film. A growing nanorod is highlighted by the yellow dotted line which could be at its early stage of nucleation and growth. **b** A cross-sectional SEM image of a vertically grown nanorods. Scale bars in **a** and **b** 200 nm.

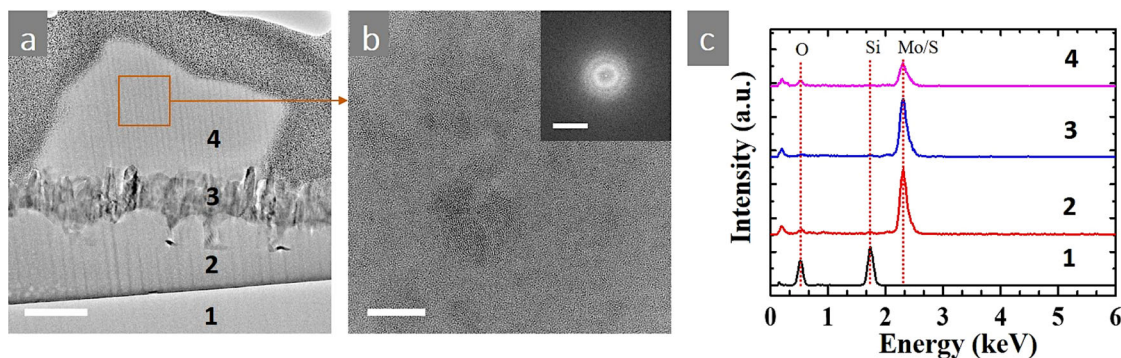


Fig. 3 Microstructure of the nanorods. **a** A bright field cross-sectional TEM image indicating four regions. Scale bar 100 nm. **b** HRTEM image collected from region 4. Scale bar 10 nm. A corresponding FFT image is shown in the inset. Scale bar 10 1/nm. The EDS analysis shown in **c** reveal the chemical composition of the four regions. 1: SiO₂ region, 2: Mo thin film region; including some oxygen content, 3: MoS₂ NSs region, 4: nanorod region, containing Mo and oxygen.

(Mo) and oxygen (O) constitute the main chemical contents of the nanorods.

Moreover, Raman spectroscopy was conducted on the pristine and aged samples. Strong Raman peaks E_{2g}¹ and A_{1g}, corresponding to common MoS₂ vibration modes, were observed for both samples (Fig. 4).

However, for the aged sample, additional small peaks at various locations are also recorded. Based on the typical vibration modes of MoS₂, the obtained extra vibrational peaks are ascribed to MoO₃ structure (Table 1).

Interestingly, it is also observed that the difference in Raman shifts between the main MoS₂ peaks, i.e., $\Delta\omega$ (E_{2g}¹–A_{1g}), for the pristine sample is 25.2 cm⁻¹, whereas for the aged sample it turns to $\Delta\omega = 26.8$ cm⁻¹. This infers that the thickness of MoS₂ NSs has increased, which is coherent with the vertical shape growth. A throughout theoretical and experimental investigation on the Raman shifts and MoS₂ orientation relationship can be found here²⁶.

In addition, a blue shift is also observed for the aged specimen, indicating a strain relaxation occurring in the sample due to the long-term aging. This indicates that during the aging, MoS₂ NSs have released some of their internal stresses that could be at the origin of the nanorods formation after long-term aging. The changes in Raman shifts induced by thermal annealing have been systematically investigated in more details on the MoS₂ monolayer²⁷, these authors linked the changes in Raman shifts to the increasing defects. Similar observations have been also reported for GaN²⁸ and SiGe²⁹ strained samples. Using Tsang's model³⁰, we have utilized the Raman shifts values to determine the induced strains, respectively in porous GaN and in aged SiGe. The calculated strains by this method were supported by other investigations such as X-ray diffraction and nano-indentation. Additionally, the intensity ratio of E_{2g}¹/A_{1g} is found to increase with aging, indicating the higher vibrations in the out-of-plane direction, which is coherent with the nanorods formation from MoS₂ NSs.

Finally, XPS measurements were carried out to analyze induced changes in the sample's surface chemistry following the long-term exposure to air and humidity. Figure 5 shows the XPS results obtained for the pristine and aged samples.

A small peak at 235.7 eV, corresponding to Mo_{3d}, suggests the presence of MoO₃ traces in the pristine sample. Its intensity is significantly increased in the aged sample, which correlates with the observed MoO₃ Raman peaks. S_{2p} spectra for both, pristine and aged samples, are the common characteristic peaks at ~162 and ~163 eV. Nevertheless, an additional peak appears at 168.7 eV for the aged sample, which corresponds to the S–O group. O_{1s} spectra in both cases show the characteristic peak at ~532 eV with an additional peak at ~530 eV corresponding to MoO₃. The intensity of this peak is highly increased for the aged sample. XPS

Table 1. Raman shifts peak positions with respect to MoO₃ and S vibrational modes in the 250–500 cm⁻¹ frequency range.

Raman shifts peak positions	MoO ₃ vibrational modes	S vibrational modes
288.9 cm ⁻¹	282 (B _{3g} -δ)	439
338.7 cm ⁻¹	335 (A _g -δ)	
365.4 cm ⁻¹	377	
489.4 cm ⁻¹	469 (B _{1g} -ν)	473

Bold values correspond to indexed vibrational frequencies of MoO₃ and S.

results clearly point toward a pronounced role of oxygen reaction with Mo and S in the aged sample. As it can be seen, the intensity of both 235.6 and 530.1 eV peaks associated with MoO₃ is higher for the aged MoS₂ sample, suggesting the oxidation of MoS₂ during the long-term aging. Similarly, it is also recorded in the aged sample that the intensities ratio of MoO₃ and S–O groups is high, which indicates a favored oxidation of MoS₂ NSs during the aging process.

Nanorods growth mechanism

It has been reported that MoS₂ flakes could undergo an oxidation leading to the formation of white speckles when exposed to ambient air containing oxygen and moisture¹². It is also assumed that the oxidation process of the MoS₂ sites can take place at structural defects. Indeed, grain boundaries and point defects usually exhibit higher amount of dangling bonds promoting the oxidation and degradation of MoS₂ samples^{13,19}.

In this study, the vertically grown MoS₂ NSs have a large number of exposed edges. Those edges are likely to retain a high degree of dangling bonds highly susceptible for oxidation. In general, the oxidation process results in the formation of SO₂ and MoO₃, as shown by the equation below:



In fact, SO₂ is a volatile compound, which can easily evaporate and disappear from oxidation sites. Nonetheless, XPS results showed a trace of few remaining S–O bonds on the aged sample. On the other hand, MoO₃ compound is a nonvolatile product, which remains on nucleation sites as a solid material, leading to the growth of nanorods. Their growth up to few microns in length during the 36 months aging period is an indication of the continuous quality and consistency of the oxidation process.

Based on experimental evidence, we analyze the microscopic origin of the nanorods formation as a major consequence of the

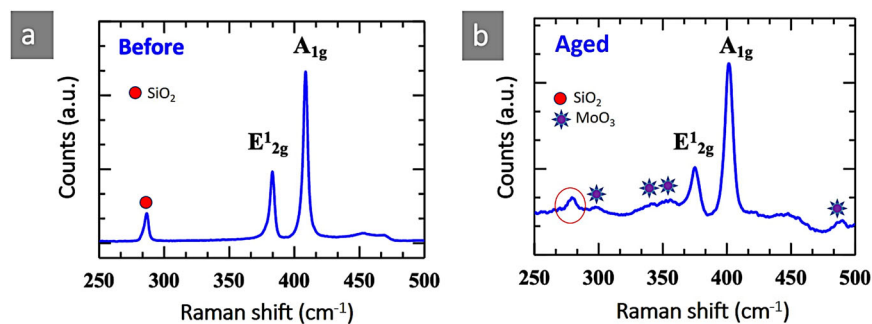


Fig. 4 Samples vibrational characterization before and after aging. **a** Typical Raman spectra of a grown MoS₂ sample (pristine). **b** Raman spectra of the long-term aged sample (36 months).

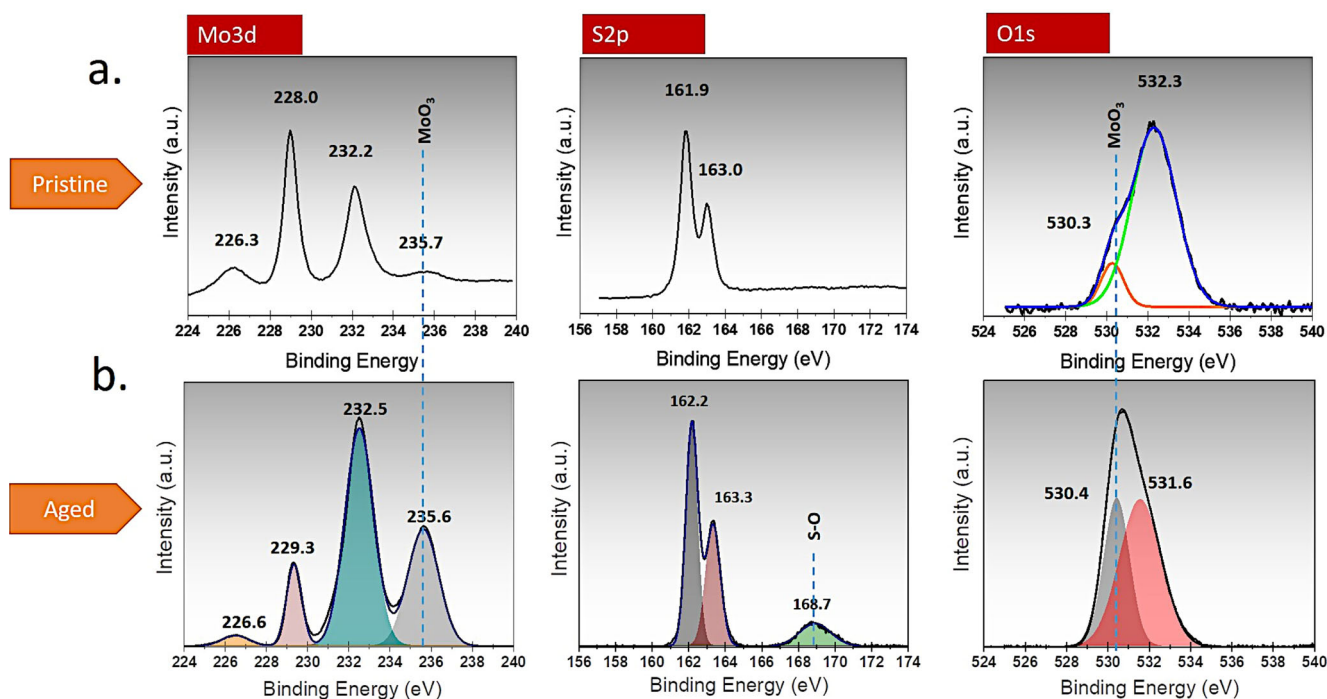


Fig. 5 XPS investigations of the pristine and long-term aged sample. **a** Mo_{3d}, S_{2p} and O_{1s} peaks shown respectively from left to right, for the pristine sample. **b** Same peaks shown for the aged sample (~36 months).

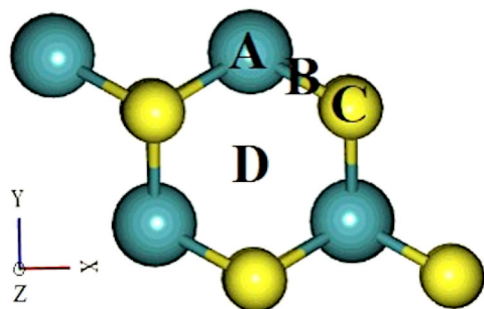


Fig. 6 MoS₂ monolayer configuration. Primary sites considered to position the adsorbents on the MoS₂ monolayer.

long-term aging process through exposure to oxygen and humidity. In fact, during the initial growth process of the vertically oriented pristine NSs, S is introduced in the CVD chamber to diffuse into the Mo thin film to form vertical MoS₂

NSs. Eventually, there is a competition in the process of diffusion of S in the Mo region and the formation of NSs. At some point, the formation of NSs could hinder S atoms from diffusing further into the Mo region, which leaves parts of the Mo region intact. Finally, continuously and homogeneously distributed NSs on top of the Mo region could occur. However, even though MoS₂ NSs are observed to be continuous, very small gaps among the NSs form nanoscopic paths for the undisturbed Mo region to interact at low kinetics with the oxygen present in the atmosphere during the long-term aging. This process could lead to the formation of oxygen enriched Mo nanorods. The natural nucleation and growth of oxygen enriched Mo nanorods is expected to be very slow as the size of the nanorods does not change during weeks. Moreover, the presence of very short nanorods (length of the order few tens of nm) is also observed (shown by the dotted line in Fig. 2a) which is assumed to be in the early stage of its growth. This indicates that the formation of new nanorods could be maintained as long as there is pristine Mo beneath the MoS₂ NSs.

Table 2. Fully relaxed distances for the oxygen (O₂) on top of MoS₂ monolayer in different positions.

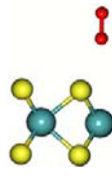
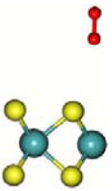

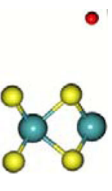
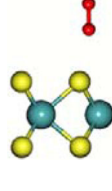
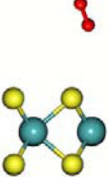
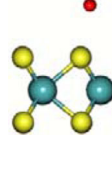
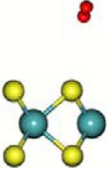
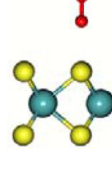
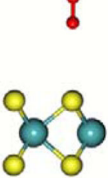
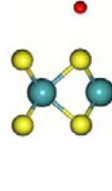
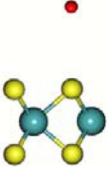
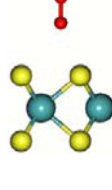
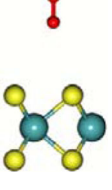
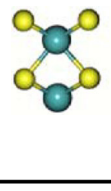
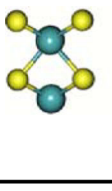
Position	Before optimization	After optimization
O ₂ _V@A		
O ₂ _H@A		
O ₂ _V@B		
O ₂ _H@B		
O ₂ _V@C		
O ₂ _H@C		
O ₂ _V@D		

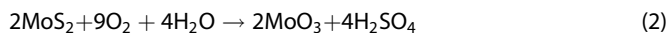
Table 2 continued

Position	Before optimization	After optimization
O ₂ _H@D		

V vertical, H horizontal.

DFT calculations

To further examine the stability and chemical surface reactivity of MoS₂ monolayers with O₂ and H₂O under ambient conditions, we have performed thermodynamic and DFT calculations on oxidized MoS₂ in dry and humid air using Eq. (1) and the following equation³¹:



The geometrical configuration of adsorbents on top of the MoS₂ monolayer plays an important role in favoring Mo oxidation processes. To evaluate this effect, we have positioned O₂ and H₂O as adsorbents at four different potential initial sites of the MoS₂ supercell, as shown in Fig. 6.

Adsorbent was considered as follow: on top of the Mo at site A, on top of the Mo-S bond at site B, on top of S at site C, and at the center of the hexagon at site D. For each configuration we let the system relax until reaching the minimum energy.

After stabilization of adsorbents (O₂ and H₂O gas molecules) at the considered positions with minimum energy requirements, the obtained configurations are further used to conduct a theoretical study of their adsorption behaviors on pristine MoS₂ monolayer via first-principles calculations³².

Adsorbed O₂ and H₂O molecules are constructed by positioning a specific gas molecule vertically and horizontally (parallel) to the surface of the compound, as detailed in Tables 2 and 3, respectively. The distance between the MoS₂ surface and first atoms of the gas molecules was set to 2.5 Å before optimization.

Using first-principles calculations, we examine the reaction of MoS₂ surface with the considered gas molecules, where adsorption energies E_{ad} are calculated using the following relation^{33,34}:

$$E_{\text{ad}} = E_{\text{MoS}_2 + \text{molecule}} - E_{\text{MoS}_2} - E_{\text{molecule}} \quad (3)$$

where $E_{\text{MoS}_2 + \text{molecule}}$ is the total energy of MoS₂ with the adsorbed gas molecule, E_{MoS_2} , and E_{molecule} are the total energies of pristine MoS₂ and isolated gas molecule, respectively. A positive value of the adsorption energy indicates that the adsorption is endothermic, meaning that the reaction is energetically unfavorable. In contrast, a negative value of the adsorption energy corresponds to an exothermic reaction, which is energetically favorable. Table 4 summarizes DFT calculation results including adsorption energies (E_{ad}) angles, bond lengths and distances between the gas molecule and MoS₂ surface for different configurations. Results show that adsorption energies are negative for either O₂ or H₂O in all considered configurations. This indicates that all reactions are most likely to occur. Moreover, our findings revealed that H₂O molecules achieved a lowest absolute $E_{\text{ad}} = -0.10$ eV at the vertical position B compared to $E_{\text{ad}} = 1.09$ eV for O₂ molecules at practically all positions (i.e., Table 4).

After adsorption on the MoS₂ surface, molecules show some deformations at the vicinity of Mo atoms leading to the formation of MoO₃ at almost all possible positions. Hence, our DFT

Table 3. Fully relaxed distances for water vapor (H_2O) on top of MoS_2 monolayer in different positions.

Position	Before optimization	After optimization
MOS_2_V@A		
MOS_2_H@A		
MOS_2_V@B		
MOS_2_H@B		
MOS_2_V@C		
MOS_2_H@C		
MOS_2_V@D		

Table 3 continued

Position	Before optimization	After optimization
MOS_2_H@D		

V vertical, H horizontal.

calculations indicate a fair agreement with the conclusions stated from experimental measurements. Specifically, aging of MoS_2 NSs in ambient conditions is primarily a Mo oxidation-dependent process, resulting in the formation of MoO_3 compound. The highly favored O_2 reaction, at all possible sites, compared to H_2O as revealed by the DFT calculations³⁴, supports our analysis and interpretation of the microscopic aging mechanism. That is, the aging-dependent oxidation is a continuous process at intact Mo nanoscopic sites resulting from the initial growth mechanism of MoS_2 NSs. The originality in this work consisted in observing a random growth of merely MoO_3 nanorods, which has been made possible by the large extension of the aging period beyond the 18 months cap, as previously reported in literature. The present results suggest the possibility of even further structural and morphological changes to be induced on MoS_2 samples for even longer aging periods, which would result from prolonged oxidation processes.

Furthermore, we have conducted accelerated aging experiments inside electron microscope (see Supplementary Note). The experiments consist of time-lapse assessment of the MoS_2 film/ MoO_3 nanorods degradation under electron beam irradiation. These experiments provide an important outlook of a potential temperature induced aging/degradation of MoS_2 - MoO_3 when used in harsh environments.

It is worth noticing that the MoS_2 - MoO_3 composite materials has various potential applications in charge storage²⁰, gas sensing²¹, and electromagnetic wave absorption²². Given the promising nature of this composite and these associated technological applications, its stability under various environments is of significant impact. In this regard, our accelerated aging experiments provide further valuable insights into the unstable nature of such composites when used under harsh environments.

DISCUSSION

Alternatively, it is necessary to look for solutions aiming to mitigate the MoS_2 degradation. In this work, O_2 and H_2O are identified to have a deleterious effect on MoS_2 long-term stability. An obvious approach to slow down the aging process, consists to handle the MoS_2 samples in inert atmosphere at reduced relative humidity, such as in glove box during the manipulation and in a desiccator for storage. The samples/devices could also be stored in vacuum to avoid the aging process. In certain applications, where there will be an inherent exposure of the MoS_2 flakes/edges to the environment, an encapsulating layer such as, polymer layer with 10–20 nm could be deposited to avoid such degradation as reported elsewhere¹³. Although, a conformal deposition throughout the sample could be a challenge due to the presence of

Table 4. Adsorption energies and orientations of adsorbents in the four positions considered.

Position	Gas	V/H	Angle (°)		Bond lengths (Å)		$d_{\text{MoS}_2\text{-gas}}$ (Å)		E_{ad} (eV)
			Before	After	Before	After	Before	After	
A	H ₂ O	V	105.36	104.30	1	0.97–0.98	2.5	2.52	–0.08
		H		104.36		0.98		3.19	–0.09
	O ₂	V	–	–	1.23	1.24	2.5	3.50	–1.09
		H				1.24		3.62	–1.09
B	H ₂ O	V	105.36	104.59	1	0.98–0.97	2.5	2.72	–0.10
		H		104.33		0.97		3.40	–0.09
	O ₂	V	–	–	1.23	1.24	2.5	3.79	–1.09
		H				1.24		3.57	–1.09
C	H ₂ O	V	105.36	104.87	1	0.97–0.98	2.5	2.74	–0.09
		H		104.50		0.97		3.99	–0.07
	O ₂	V	–	–	1.23	1.24	2.5	3.79	–1.09
		H				1.24		3.94	–1.09
D	H ₂ O	V	105.36	104.28	1	0.97–0.98	2.5	2.52	–0.08
		H		104.37		0.98		3.30	–0.08
	O ₂	V	–	–	1.23	1.24	2.5	3.53	–1.09
		H				1.24		3.51	–1.09

V vertical, H horizontal.

vertical edges, some tools could achieve a good result such as evaporators and dip coaters.

In summary, the long-term aging (~36 months) of CVD grown 2D MoS₂ thin film has been investigated. Degradation of the grown material in terms of several morphological and chemical changes such as, oxidation of the MoS₂ sheets, formation of nanorods of few nm to few microns, relaxation of the MoS₂ sheets is observed. Nanorods are composed of MoO₃ as demonstrated by Raman, XPS and EDS studies. DFT calculations demonstrated that atmospheric H₂O and O₂ can participate in the reaction with MoS₂ to induce chemical changes in the material. However, reactions with O₂ were found more favorable. Additionally, we demonstrated that nanorods could undergo a transformation from amorphous to crystalline form under intense electron beam irradiation and heating, which indicated the possibility of accelerated aging. Our work offers an original understanding of the extended aging mechanism of MoS₂ nanostructures exposed to ambient and humid conditions. The findings presented here provide fundamental assets for nano-engineering strategies of MoS₂-based devices in view of their stability over time and operating life cycle.

METHODS

Sample growth

MoS₂ was grown on SiO₂/Si substrate using a double sulfurization process. Initially a ~50 nm Mo thin film was deposited on the substrate using a sputter system. Sulfurization is performed at ambient pressure in a CVD system. Details of the sample growth are discussed in our earlier article⁹. The sample was then exposed to laboratory ambient conditions, i.e., room temperature at an average relative humidity of 40%, for a period of ~36 months.

Microstructural characterization

To investigate the morphology of the MoS₂ aged samples, a dual beam system consisting of a scanning electron microscope (SEM) and a focused ion beam (FIB) Helios 650 Thermo Fisher Scientific™

was used. A typical voltage of 5 kV and beam current of 100 pA was used for the SEM imaging. The Elstar electron column was operated in ultra-high-resolution with magnetic immersion and field free mode. The tool was also used to prepare cross-sectional samples and thin lamellas for TEM measurements. Lamellas were prepared using standard FIB lift-out technique³⁵. Initially, a protective layer of Pt material was made on top of the MoS₂ flakes using successively electron beam and ion beam deposition. The dimension of the deposited layer was 20 μm × 2 μm × 2 μm in size. Subsequently, regular cross section and cleaning cross section methods were implemented and a rectangular slice of 20 μm × 1 μm × 6 μm was prepared. Next, the prepared thin slice was fetched (lift out) using a micromanipulator and placed on a Cu TEM grid for further thinning. Ion beam having energy of 30 keV and current of 0.43–0.79 nA was used for rough thinning and beam energy of 5 keV and beam current of 41 pA was implemented for final thinning. At the end of the thinning process, the thickness of TEM lamella was below 80 nm.

Analytical characterization

TEM investigations and EDS analyses of the samples were conducted using an image corrected TEM system Titan G2 Thermo Fisher Scientific™. The operating voltage was set to 300 kV throughout the investigation. Raman spectroscopy Horiba™ was used to characterize the chemical bonds and vibrational states using a green laser excitation (532 nm). X-ray photoelectron spectroscopy (XPS) study was carried out using a Thermo Fisher Scientific™ K-alpha spectrometer and a PHI VersaProbe III scanning XPS microprobe. The spectroscopes possess a monochromatic and microfocused Al K-Alpha X-ray source (1486.6 eV). The X-ray beam power was kept at ~50 W. During the experiment, E-neutralizer (1 V), and I-neutralizer (0.11 kV Ar⁺ ion) were implemented. The obtained peaks were corrected using the C 1s as reference at 284.6 eV. The peaks were further analyzed using MultiPak and OriginPro programs.

Density functional theory simulations

The computational calculations are based on the DFT using generalized gradient approximation with the Perdew-Burke-Ernzerhof exchange-correlation functional³⁶, implemented in the open-source software Quantum ESPRESSO^{37,38}.

A 2×2 supercell of monolayer MoS₂ was used as the computational model to understand the nature of the interaction of O₂ and H₂O molecules with the surface of the two-dimensional monolayer. To address the interaction between two adjacent MoS₂ monolayers, a vacuum space of 10 Å along the c direction was implemented in calculations. All structures were fully relaxed using Broyden-Fletcher-Goldfarb-Shanno method until the maximum Hellmann-Feynman force acting on each atom was smaller than 10^{-3} Ryd/Bohr for all structures. The cutoff wave function and cutoff charge densities were 60 and 600 Ryd, respectively. These cut-off energies were determined after a convergence analysis. A ($2 \times 2 \times 1$) k-point was used in the structure optimization and total energy calculations.

DATA AVAILABILITY

Data would be made available upon request to the corresponding author.

Received: 28 June 2022; Accepted: 18 August 2022;

Published online: 06 September 2022

REFERENCES

1. Yue, Q. et al. Mechanical and electronic properties of monolayer MoS₂ under elastic strain. *Phys. Lett. A* **376**, 1166–1170 (2012).
2. Peng, Q. & De, S. Outstanding mechanical properties of monolayer MoS₂ and its application in elastic energy storage. *Phys. Chem. Chem. Phys.* **15**, 19427–19437 (2013).
3. Splendiani, A. et al. Emerging photoluminescence in monolayer MoS₂. *Nano Lett.* **10**, 1271–1275 (2010).
4. Deokar, G. et al. Large area growth of vertically aligned luminescent MoS₂ nanosheets. *Nanoscale* **9**, 277–287 (2017).
5. Cho, S.-Y. et al. Highly enhanced gas adsorption properties in vertically aligned MoS₂ layers. *ACS Nano* **9**, 9314–9321 (2015).
6. Pak, J. et al. Enhancement of photodetection characteristics of MoS₂ field effect transistors using surface treatment with copper phthalocyanine. *Nanoscale* **7**, 18780–18788 (2015).
7. Zhang, E. et al. Tunable charge-trap memory based on few-layer MoS₂. *ACS Nano* **9**, 612–619 (2015).
8. Stephenson, T., Li, Z., Olsen, B. & Mitlin, D. Lithium ion battery applications of molybdenum disulfide (MoS₂) nanocomposites. *Energy Environ. Sci.* **7**, 209–231 (2014).
9. Deokar, G. et al. Toward the use of CVD-grown MoS₂ nanosheets as field-emission source. *Beilstein J. Nanotechnol.* **9**, 1686–1694 (2018).
10. Zhang, X. et al. Two-dimensional MoS₂-enabled flexible rectenna for Wi-Fi-band wireless energy harvesting. *Nature* **566**, 368–372 (2019).
11. Roberts, E. W. Ultralow friction films of MoS₂ for space applications. *Thin Solid Films* **181**, 461–473 (1989).
12. Budania, P. et al. Long-term stability of mechanically exfoliated MoS₂ flakes. *MRS Commun.* **7**, 813–818 (2017).
13. Gao, J. et al. Aging of transition metal dichalcogenide monolayers. *ACS Nano* **10**, 2628–2635 (2016).
14. Şar, H. et al. Long-term stability control of CVD-grown monolayer MoS₂. *Phys. Status Solidi Rapid Res. Lett.* **13**, 1–7 (2019).
15. Yao, K. et al. Rapid ambient degradation of monolayer MoS₂ after heating in air. *2D Mater.* **7**, 15024 (2019).
16. Zhang, X., Jia, F., Yang, B. & Song, S. Oxidation of molybdenum disulfide sheet in water under in situ atomic force microscopy observation. *J. Phys. Chem. C* **121**, 9938–9943 (2017).
17. Qiu, H. et al. Electrical characterization of back-gated bi-layer MoS₂ field-effect transistors and the effect of ambient on their performances. *Appl. Phys. Lett.* **100**, 123104 (2012).
18. Lince, J. R., Loewenthal, S. H. & Clark, C. S. Tribological and chemical effects of long term humid air exposure on sputter-deposited nanocomposite MoS₂ coatings. *Wear* **432–433**, 202935 (2019).
19. Chen, X. et al. Degradation behaviors and mechanisms of MoS₂ crystals relevant to bioabsorbable electronics. *NPG Asia Mater.* **10**, 810–820 (2018).
20. Joseph, N. & Bose, A. C. One pot synthesis of MoO₃/MoS₂ composite and investigation on its electrochemical charge storage properties. *AIP Conf. Proc.* **2115**, 030551 (2019).
21. Singh, S., Deb, J., Sarkar, U. & Sharma, S. MoS₂/MoO₃ nanocomposite for selective NH₃ detection in a humid environment. *ACS Sustain. Chem. Eng.* **9**, 7328–7340 (2021).
22. Li, C.-Q., Shen, X., Ding, R.-C. & Wang, G.-S. Controllable synthesis of one-dimensional MoO₃/MoS₂ hybrid composites with their enhanced efficient electromagnetic wave absorption properties. *Chempluschem* **84**, 226–232 (2019).
23. Lei, Y., Yang, X. & Feng, W. Synthesis of vertically-aligned large-area MoS₂ nanofilm and its application in MoS₂/Si heterostructure photodetector. *Nanotechnology* **33**, 105709 (2021).
24. Barzegar, M., Irajizad, A. & Tiwari, A. On the performance of vertical MoS₂ nanoflakes as a gas sensor. *Vacuum* **167**, 90–97 (2019).
25. Rajput, N. S., Sloyan, K., Anjum, D. H., Chiesa, M. & Ghaferi, A. A user-friendly FIB lift-out technique to prepare plan-view TEM sample of 2D thin film materials. *Ultramicroscopy* **235**, 113496 (2022).
26. Zhao, Y. et al. Raman spectroscopy of dispersive two-dimensional materials: a systematic study on MoS₂ solution. *J. Phys. Chem. C* **124**, 11092–11099 (2020).
27. Kim, H. J. et al. Changes in the Raman spectra of monolayer MoS₂ upon thermal annealing. *J. Raman Spectrosc.* **49**, 1938–1944 (2018).
28. Najar, A., Gerland, M. & Jouiad, M. Porosity-induced relaxation of strains in GaN layers studied by means of micro-indentation and optical spectroscopy. *J. Appl. Phys.* **111**, 093513 (2012).
29. Ravoux, F. et al. Effect of rapid thermal annealing on crystallization and stress relaxation of SiGe nanoparticles deposited by ICP PECVD. *RSC Adv.* **7**, 32087–32092 (2017).
30. Tsang, J. C., Mooney, P. M., Dacol, F. & Chu, J. O. Measurements of alloy composition and strain in thin Ge_xSi_{1-x} layers. *J. Appl. Phys.* **75**, 8098–8108 (1994).
31. Szoszkiewicz, R. Local interactions of atmospheric oxygen with MoS₂ crystals. *Materials* **14**, 5979 (2021).
32. Kotbi, A., Hartiti, B., Fadili, S., Ridah, A. & Thevenin, P. Experimental and theoretical studies of CuInS₂ thin films for photovoltaic applications. *J. Mater. Sci. Mater. Electron.* **30**, 21096–21105 (2019).
33. Zuo, H. W. et al. Pt₄ clusters supported on monolayer graphitic carbon nitride sheets for oxygen adsorption: a first-principles study. *Wuli Huaxue Xuebao/Acta Phys. Chim. Sin.* **32**, 1183–1190 (2016).
34. Yue, Q., Shao, Z., Chang, S. & Li, J. Adsorption of gas molecules on monolayer MoS₂ and effect of applied electric field. *Nanoscale Res. Lett.* **8**, 425 (2013).
35. Rajput, N. S. et al. Electron beam induced rapid crystallization of water splitting nanostructures. *MRS Adv.* **1**, 825–830 (2016).
36. Perdew, J. P., Burke, K. & Ernzerhof, M. Generalized gradient approximation made simple (vol 77, pg 3865, 1996). *Phys. Rev. Lett.* **78**, 1396–1396 (1997).
37. Mouloua, D. et al. Recent progress in the synthesis of MoS₂ thin films for sensing, photovoltaic and plasmonic applications: a review. *Materials* **14**, 3283 (2021).
38. Kotbi, A. et al. Graphene and g-C₃N₄-based gas sensors. *J. Nanotechnol.* **2022**, 20 (2022).

ACKNOWLEDGEMENTS

This study was funded by an internal seed grant provided by the Masdar Institute of Science and Technology and University of Picardie Jules Verne (M.J.). Authors are thankful to Dr. G. Deokar for providing the samples.

AUTHOR CONTRIBUTIONS

N.S.R. and M.J. conceived the study; N.S.R. and K.K. carried out the experimental study; A.K. performed the modeling. N.S.R., A.K. and M.J. analyzed the data. All authors contributed equally on writing, editing, and reviewing the manuscript.

COMPETING INTERESTS

The authors declare no competing interests.

ADDITIONAL INFORMATION

Supplementary information The online version contains supplementary material available at <https://doi.org/10.1038/s41529-022-00288-4>.

Correspondence and requests for materials should be addressed to Mustapha Jouiad.

Reprints and permission information is available at <http://www.nature.com/reprints>

Publisher's note Springer Nature remains neutral with regard to jurisdictional claims in published maps and institutional affiliations.



Open Access This article is licensed under a Creative Commons Attribution 4.0 International License, which permits use, sharing, adaptation, distribution and reproduction in any medium or format, as long as you give

appropriate credit to the original author(s) and the source, provide a link to the Creative Commons license, and indicate if changes were made. The images or other third party material in this article are included in the article's Creative Commons license, unless indicated otherwise in a credit line to the material. If material is not included in the article's Creative Commons license and your intended use is not permitted by statutory regulation or exceeds the permitted use, you will need to obtain permission directly from the copyright holder. To view a copy of this license, visit <http://creativecommons.org/licenses/by/4.0/>.

© The Author(s) 2022, corrected publication 2021